Competition of pattern forming instabilities due to phase front curvature in an optical system

F. Huneus* and W. Lange†
Institut für Angewandte Physik, Westfälische Wilhelms–Universität Münster, Corrensstr. 2/4, D–48149 Münster, Federal Republic of Germany‡

T. Ackemann§
Department of Physics, University of Strathclyde, John Anderson Building, 107 Rottenrow, Glasgow G4 ONG, United Kingdom‖
(Received 4 October 2005; published 18 January 2006)

In this paper we analyze experimentally and theoretically the competition between two pattern forming instabilities in a single mirror feedback scheme with sodium vapor as the nonlinear medium. Two types of structures with different transverse wave numbers are observed experimentally, if the spatial phase modulation of the light field is varied. This phenomenon results from the combination of a nonlinear self-lensing effect on the one hand and of the externally controlled phase front curvature of the light field on the other. A linear stability analysis yields two instabilities whose length scales match quite well the experimental findings. Further analysis reveals the mechanism of length-scale selection in this system and demonstrates the possibly crucial role of phase front curvature in optical pattern formation.

DOI: 10.1103/PhysRevE.73.016215 PACS number(s): 89.75.Kd, 89.75.Fb, 42.65.Sf

I. INTRODUCTION

An intriguing feature of spontaneous pattern formation is the appearance of structures such as stripes, hexagons, or spirals in very different natural or laboratory systems. In particular, spirals occur, e.g., in chemical reactions [1,2] and in the chemotaxis of some biological specimens [3,4]. Other examples are electrochemistry [5], electro-luminescence of thin films [6], heterogeneous catalysis [7], Faraday experiments, and convection instabilities [8].

In optics, a lot of attention was drawn to spiral structures in the phase of the optical field, so-called "optical vortices" (e.g., [9–11]). Here, the phase change on a circle is an integer multiple of 2π while in the center the phase is singular and the intensity is zero. As the spirals are only formed in the phase of the electro-magnetic field these structures cannot be observed by the eye directly.

This feature is different from spiral structures occurring in the amplitude of the light field. Such *intensity* spirals are much less studied in optics. They were predicted to be generated in a secondary bifurcation in an internally pumped optical parametric oscillator [12] and they have been observed in nonlinear feedback systems in which the rotational symmetry is broken by a rotation of the feedback loop [13–15] as well as in a single-mirror scheme with sodium vapor as the nonlinear medium and rotationally symmetric feedback [16,17]. In the latter case it has been proven experimentally that the existence of a phase front curvature in the light field was essential in the formation of dynamic target patterns and of the spirals. Very recently, the importance of a phase front curvature in the formation of intensity spirals has also been emphasized in an optically driven semi-conductor microresonator [18]. In [16,18], it was found that the direction of rotation of the spirals could be inverted by changing the phase front curvature. While in [18] a phase front curvature was applied externally, it was self-induced in [16].

In this paper we present an analysis of the occurrence of target patterns in the single-mirror feedback experiment with sodium vapor as the nonlinear medium. We demonstrate that the competition between different pattern forming instabilities can drastically be influenced by the existence of a phase front curvature and discuss the implications. These include the formation of intensity spirals which are considered as disturbed target patterns.

II. EXPERIMENTAL SETUP

The considered system is a realization of the well-known single-mirror feedback scheme that was analyzed in [19–21]. Sodium vapor in a nitrogen buffer gas atmosphere is used as the nonlinear medium.

Figure 1 shows a schematic of the experimental setup. A frequency-stabilized dye laser serves as the light source. The laser frequency is tuned to 10 to 15 GHz above the sodium D_1 transition. The intensity is adjusted by means of an electro-optical modulator. Spatial filtering of the light field by use of a single-mode optical fiber yields a smooth Gaussian-shaped intensity profile. The phase front curvature of the laser beam is addressed by a combination of two telescopes. The longitudinal shift (Δx) of the first lens of the first telescope, L_1, controls the curvature of the phase fronts at the position of the second lens, L_2, of the first telescope. The second telescope (L_3 and L_4) images the output facet of the first telescope onto the vapor without modifying the phase distribution. In this way we can vary the phase front curvature of the light field continuously without major changes of the beam radius. Figure 2 shows the radius of the phase front

*Electronic address: huneus@uni-muenster.de
†Electronic address: w.lange@uni-muenster.de
‡http://www.uni-muenster.de/Physik/AP/Lange/Welcome-e.html
§Electronic address: thorsten.ackemann@strath.ac.uk
‖http://www.photonics.phys.strath.ac.uk/

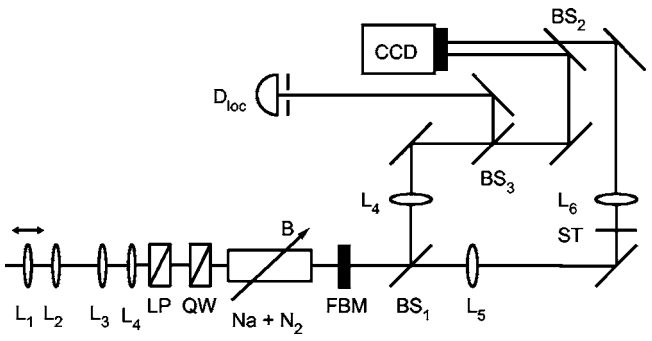

FIG. 1. Schematic experimental setup. LP: linear-polarizer, QW: quarter-wave plate, L_1 to L_6: lenses, FBM: feedback mirror, B: magnetic field, BS_1, BS_2, BS_3: beam splitters, ST: stop.

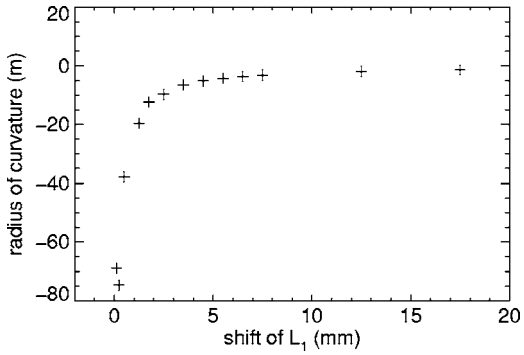

FIG. 2. Radius of phase front curvature in dependency on the shift of L_1.

curvature of the light field at the position of the nonlinear medium in dependency on the shift of L_1. We concentrate our investigations on positive values of Δx because they introduce the phase front curvature of a convergent beam which is needed to counteract the phase modulation that is nonlinearly induced by the Gaussian-shaped intensity profile of the laser beam [16]. Immediately before the light enters the sodium vapor its polarization state is adjusted to be circular by a combination of a linear polarizer and a quarter-wave plate. In the sodium vapor the beam radius at the $1/e^2$ point of intensity is approximately 1.5 mm.

The sodium vapor is contained in a cell which is surrounded by three orthogonal pairs of Helmholtz coils. By this setup one can compensate for the earth's magnetic field or can create an oblique dc magnetic field that changes the optical properties of the vapor. The sodium cell is heated to $T_{cell} \approx 340\ ^\circ\mathrm{C}$. The pressure of the nitrogen buffer gas atmosphere is 300–310 hPa.

After passing the short sodium vapor cell (length 15 mm) the light propagates to a feedback mirror which is located in the beam path at a distance d (typically 75 mm) behind the cell. Ninety-nine percent of the power is reflected into the nonlinear medium. The small amount of light which is transmitted by the mirror is used for the analysis of the transverse structures. The lens L_4 images the intensity distribution at a distance of $2d$ behind the mirror on one-half of the chip of a charge-coupled device (CCD) camera. This plane is chosen because here the optical field is proportional to the light reentering the nonlinear medium. In the following we call this the near-field distribution. The corresponding far field is provided by L_5 in a $2f$ scheme with the central part being blocked by a stop. L_6 images the plane of the stop onto the other half of the camera chip. The camera is equipped with an image intensifier and a fast shutter provided by a microchannel plate which allows the time-resolved acquisition of 8-bit gray-scale images 768×576 pixels in size. In another arm of the setup a photodiode is placed behind a pinhole in the image plane of L_4. Its output signal is proportional to the local intensity of a small part of the transverse cross section of the laser beam and can also be used as a trigger for the "video-sampling method" that allows the recording of slow motion sequences of fast repetitive processes by scanning the delay between a trigger signal and the image acquisition [22,23].

III. EXPERIMENTAL OBSERVATIONS

If the input power is increased in this system, dynamical target patterns and spirals with an inward motion are observed in the transverse intensity profile of the laser beam. The structures are stable for periods of time ranging from milliseconds up to some minutes. For constant experimental parameters, the system exhibits spontaneous switching between target patterns and spirals as well as spirals with varying numbers of arms or different chiralities [16].

In Fig. 3 snapshots are shown for different positions of L_1. If the beam waist is placed within the sodium vapor, i.e., for flat phase fronts of the incident light, targets and spirals are observed. Here, a three-armed spiral with a spatial frequency of 15 rad/mmis shown [Fig. 3(a)]. Such spirals with an inward radial motion of the spiral arms occur up to a shift of 2.25 mm. In Fig. 3(b) the upper half of the beam is structured by the remainder of a spiral or a target pattern while there is evidence of a shorter length scale in the lower part.

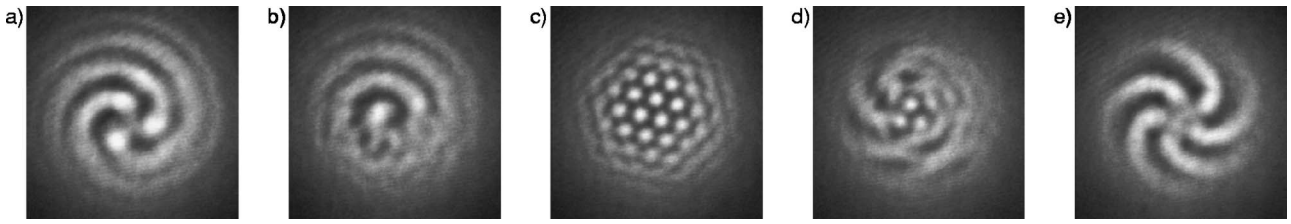

FIG. 3. Snapshots of structures spontaneously formed beyond threshold taken from an experiment in which the shift of L_1 is varied. Parameters: $d=75$ mm, $\Delta=14$ GHz, $B_\perp=3.6\ \mu$T, $B_z=24.0\ \mu$T, $T_{cell}=355\,^\circ$C, $p_{N_2}=307$ hPa; (a) $\Delta x=0$ mm, $P_{in}=186$ mW; (b) $\Delta x=2.25$ mm, $P_{in}=186$ mW; (c) $\Delta x=8$ mm, $P_{in}=162$ mW; (d) $\Delta x=12$ mm, $P_{in}=167$ mW; and (e) $\Delta x=17.5$ mm, $P_{in}=174$ mW.

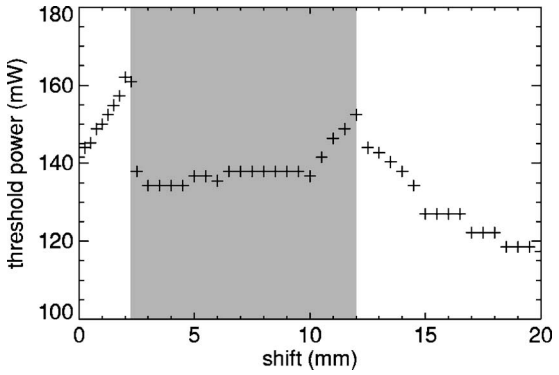

FIG. 4. Threshold intensity of spontaneous pattern formation in dependency on the shift of L_1. The gray shaded area indicates the interval in which stationary patterns with the smaller length scale and a hexagonal symmetry are observed beyond threshold. Parameters as in Fig. 3.

This length scale reappears in a nice stationary, hexagonal pattern with transverse wave number $q_{Hex} \approx 26$ rad/mm if the shift of L_1 is further increased [Fig. 3(c), $\Delta x = 8$ mm]. At $\Delta x = 12$ mm [Fig. 3(d)] we find again a structure which combines two length scales. In the beam center, three constituents remain of the hexagonal pattern with the small length scale whereas the outer parts are structured with the length scale of the spirals. Phenomenologically similar structures have been observed in a spiral core instability in Rayleigh-Bénard convection [24]. It is believed, however, that the phenomena are not closely related, since in contrast to the present case a vortex is the primary organization center of the spirals in [24]. For even larger values of the shift again spirals are generated. Their radial motion now is directed outward [Fig. 3(e), $\Delta x = 17.5$ mm].

In Fig. 4 the threshold power needed for the spontaneous formation of structures is plotted in dependency on the longitudinal shift of L_1. The gray-shaded area indicates the interval in which stationary patterns with the smaller length scale and a hexagonal symmetry are observed beyond threshold. The boundaries of this interval match with abrupt changes in the threshold power. The transition structures which show patches of both length scales exhibit higher thresholds than the "pure" structures. In contrast to theoretical expectations for the homogeneous system, we observe no interaction of the length scale belonging to the dynamical structures and the length scale belonging to the stationary pattern, neither so-called "winking hexagons" [25] nor resonant patterns like those predicted in [26].

IV. THEORETICAL MODEL

The experiments are analyzed on the basis of a semiclassical model in which the light interacts with a homogeneously broadened $J = \frac{1}{2} \leftrightarrow J' = \frac{1}{2}$ transition. This description has been proven to be adequate in several previous experiments [27–30], so that only the main features are discussed here. Details can be found in the literature [27,30,31].

Due to angular momentum selection rules, σ_+-circularly polarized light excites atoms from the $(m_J = -\frac{1}{2})$-Zeeman sublevel of the ground state. As the atoms relax into both Zeeman substates a population imbalance is created. This process is known as "optical pumping" [32]. We consider the direction of the laser beam as quantization axis (z axis). In the following we will refer to it as the "longitudinal" direction. The population difference is proportional to the longitudinal component of a macroscopic magnetization of the sodium vapor. A dc magnetic field with nonvanishing longitudinal and transverse components forces the magnetization to precess and by that it generates transverse components of the magnetization. The state of the sodium vapor can be described by a Bloch vector $\mathbf{m} = (m_x, m_y, m_z)$ that is proportional to the magnetic moment of the sample. Its dynamical evolution is given by the partial differential equation [27–29,33]:

$$\frac{\partial}{\partial t}\mathbf{m} = -\gamma \mathbf{m} + D\Delta_\perp \mathbf{m} + \hat{\mathbf{e}}_z P(m_z) - P(m_z)\mathbf{m} - \mathbf{m} \times \mathbf{\Omega}(m_z). \tag{1}$$

We define a nonlinear operator by setting

$$\frac{\partial}{\partial t}\mathbf{m} = \mathcal{N}(\mathbf{m}). \tag{2}$$

In Eq. (1) γ is a constant relaxation rate of $\mathbf{m}$ of about 1.5 s^{-1}, D is the diffusion constant of the thermal diffusion of the sodium atoms, and $\Delta_\perp$ is the transverse part of the Laplacian. $\hat{\mathbf{e}}_z$ is the unit vector in the longitudinal direction and P is the pump rate for exciting sodium atoms. It depends on m_z (see below). P is proportional to the total intensity impinging on the sodium vapor, i.e., it is proportional to the sum of the intensity of the forward beam and the intensity of the light fed back by the mirror; interference effects can be neglected due to the thermal motion of the sodium atoms. The backward-traveling beam is modified in phase and amplitude due to the optical properties of the nonlinear medium and the diffraction acting during the propagation to the mirror and back. The next term originates from the saturation of the optical pumping process. $\mathbf{\Omega}$ is a torque vector which is defined by $\mathbf{\Omega} = (\Omega_x, 0, \Omega_z - \bar{\Delta}P)$ where Ω_x and Ω_z are the Larmor frequencies corresponding to the respective components of the external magnetic field whose transverse component defines the x direction. A light-induced level shift is described by $-\bar{\Delta}P$ in the z component of $\mathbf{\Omega}$ where $\bar{\Delta}$ is the detuning of the laser suitably normalized to the width of the D_1 resonance. Obviously, the factor P in the light shift introduces a dependence of $\mathbf{\Omega}$ on m_z. The vector product describes the Larmor precession of $\mathbf{m}$ induced by a magnetic field whose z component is modified by the light shift.

The intensity-dependent optical properties of the sodium vapor are determined by the z component of the magnetization as the nonlinear susceptibility is given by

$$\chi = -\frac{N|\mu|^2}{2\epsilon_0 \hbar \Gamma_2} \frac{\bar{\Delta} + i}{\bar{\Delta}^2 + 1}(1 - m_z). \tag{3}$$

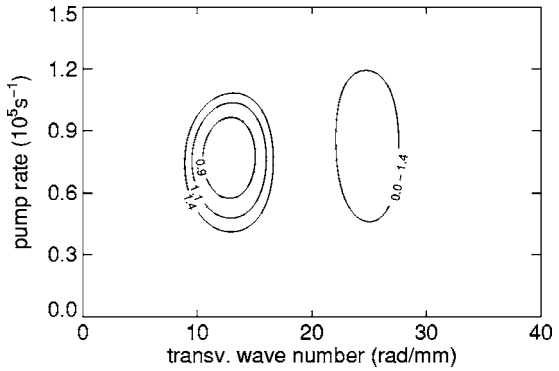

FIG. 5. Results of a linear stability analysis taking into account linear phase gradients of increasing strength (0.0, 0.3, 0.6, 0.9, 1.1, and 1.4 rad/mm). Parameters: $\Omega_x = 2.5 \times 10^5$ rad s^{-1}, $\Omega_z = 10.0 \times 10^5$ rad s^{-1}, $d = 75$ mm, $\Delta = 10.0$ GHz, $N = 0.8 \times 10^{20}$ m^{-3}, $D = 260$ mm^2 s^{-1}, $\gamma = 1.5$ s^{-1}, $\Gamma_2 = 10.1 \times 10^9$ rad s^{-1}.

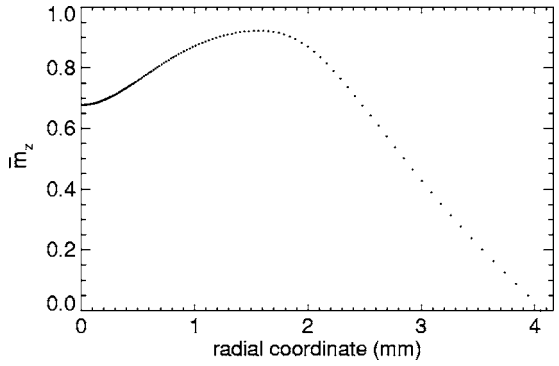

FIG. 6. Stationary, unstructured, but inhomogeneous solution nonlinearly induced by the Gaussian beam in dependency on the radial coordinate. $P = 92\,500$ s^{-1}, other parameters as in Fig. 5.

Here, N denotes the particle density of the sodium vapor, μ is the reduced dipole matrix element of the transition, and Γ_2 is the relaxation rate of the optical coherences. The spatial distribution of $\mathbf{m}$ modifies χ and this results in a spatial modulation of P imposed by the feedback beam. It is readily obtained by solving the (linear) paraxial wave equation in the free space between the sodium cell and the feedback mirror, while diffraction can be neglected in the short nonlinear medium. It is the nonlocal dependence of P on the spatial distribution of $\mathbf{m}$ that makes Eqs. (1) and (2) nonlinear.

V. LINEAR STABILITY ANALYSIS

In a linear stability analysis of the homogeneous solution of Eq. (1) a Hopf instability at a finite wave number and a stationary modulational instability at higher wave number can be found. The length scale and the frequencies of the unstable Hopf modes match nicely the experimentally observed properties of the target patterns and spirals so that the Hopf instability can be considered as the origin of these structures [16].

However, for a homogeneous phase profile of the input light field the threshold of the *stationary* modulational instability is typically lowest whereas no stationary patterns but dynamical target patterns and spirals are experimentally observed at threshold. We have proposed that this discrepancy can be attributed to the effect of the inhomogeneous phase distribution that is induced by an interplay of the Gaussian shape of the spatial intensity distribution of the laser beam and the intensity-dependent index of refraction of the sodium vapor, i.e., the nonlinearity of the medium [16].

A linear stability analysis taking into account *linear* phase gradients of various strengths illustrates the drastic influence of an inhomogeneous phase distribution on the bifurcation scenario. Figure 5 shows the instability regions of the Hopf instability and the modulational instability. At this special set of parameters the Hopf instability does not even exist without phase gradient. When the strength of the phase gradient is increased, the boundary of the modulational instability remains nearly unchanged while the Hopf instability expands its region of existence. For the largest phase gradient shown it even exhibits a lower threshold than the modulational instability.

Thus, the incorporation of the Gaussian shape of the pump profile into the theoretical treatment of the system seems to be inevitable. For a linear stability analysis, $\bar{\mathbf{m}}$, the stationary, unstructured, but inhomogeneous magnetization distribution induced by the Gaussian beam, is needed at first:

$$0 = \mathcal{N}(\bar{\mathbf{m}}(r)). \tag{4}$$

We calculate $\bar{\mathbf{m}}$ by means of Newton's method iteratively [34,35]:

$$\mathbf{m}(r)^{n+1} = \mathbf{m}(r)^n - [\nabla \mathcal{N}(\mathbf{m}(r)^n)]^{-1} \mathcal{N}(\mathbf{m}(r)^n). \tag{5}$$

Here, $\nabla\mathcal{N}$ is the Jacobian of $\mathcal{N}$. It is numerically calculated using finite differences. The strong depolarization of the sodium atoms by wall collisions are taken into account by the boundary condition $\mathbf{m}(r_0) = 0$. Here r_0 is the radius of the cell. A discretization of $\mathbf{m}$ on an orthogonal grid with $N \times N$ points would cause $\mathcal{N}$ to have $3N^2$ and $\nabla\mathcal{N}$ to have 3^2N^4 elements. As the calculations would be computationally too expensive for an appropriate choice of N, here we restrict the analysis to the rotationally symmetric problem. The pump field is given by a Gaussian beam whose beam waist is placed within the sodium vapor. To calculate the propagation of the transmitted light field the paraxial wave equation is solved in polar coordinates by a spectral algorithm using the quasi-fast Hankel-transform [35,36]. In order to use this algorithm the light field as well as the Bloch vector have to be discretized on grids with exponentially growing spacings.

Figure 6 shows the z component of the stationary, unstructured, but inhomogeneous state, $\bar{\mathbf{m}}$, in dependency on the radial coordinate. Due to the applied boundary condition the magnetization decays to zero in the outer parts. It increases towards the center until a maximum is reached. In the central region where pattern formation takes place, a dip of the magnetization is formed due to the particular shape of the nonlinear characteristic of the system [29].

To analyze the stability of $\bar{\mathbf{m}}$ we consider the eigenvalues and eigenvectors of the linearization $\nabla\mathcal{N}(\bar{\mathbf{m}})$ of the nonlinear operator $\mathcal{N}(\bar{\mathbf{m}})$. The eigenvalues of $\nabla\mathcal{N}(\bar{\mathbf{m}})$ determine the stability, the radial shape of the perturbations is given by the

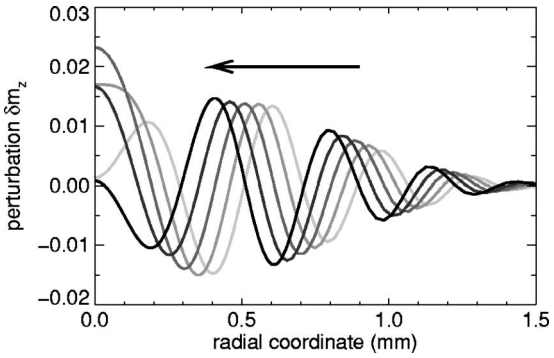

FIG. 7. Spatial shape and temporal evolution of the perturbation originating from the Hopf instability calculated for infinite radius of the input phase front curvature. Parameters as in Fig. 6.

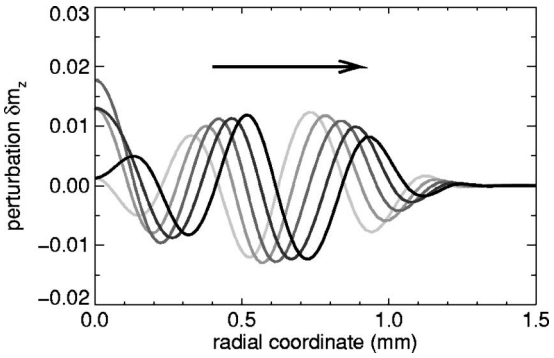

FIG. 9. Spatial shape and temporal evolution of the perturbation originating from the Hopf instability in the case of a radius of the input phase front curvature of −0.9 m. Parameters as in Fig. 6.

eigenvectors. If the pump rate P in the beam center is increased, there is a threshold at which a complex conjugate pair of eigenvalues of $\nabla\mathcal{N}(\bar{\mathbf{m}})$ crosses the imaginary axis. The system gets unstable against an oscillating spatially modulated perturbation, i.e., it undergoes a Hopf bifurcation. In Fig. 7 the spatial shape of this perturbation and its dynamical evolution are shown. The perturbation is drawn at five successive time steps with light gray denoting the first one and black the last. As it can be seen, the direction of motion is pointed towards the beam center. The dominating transverse wave vector is 15.5 rad/mm and the Hopf frequency calculated by the imaginary part of the eigenvalue is approximately 110 kHz. The amplitude of the spatio-temporal oscillation is largest in the beam center and decreases towards the boundary. Here, only the inner part of the beam profile up to a radius of 1.5 mm is displayed. As the perturbation is rotationally symmetric it is equivalent to an inwardly moving target pattern. The described features—the Hopf bifurcation itself, its length scale and frequency, and the direction of the radial motion—are in good agreement with experimental observations.

In order to understand the influence of the phase front curvature, we take into account an appropriate spatial phase distribution of the pump light. In Fig. 8 the positive real parts of the eigenvalues are plotted in dependency on the radius of

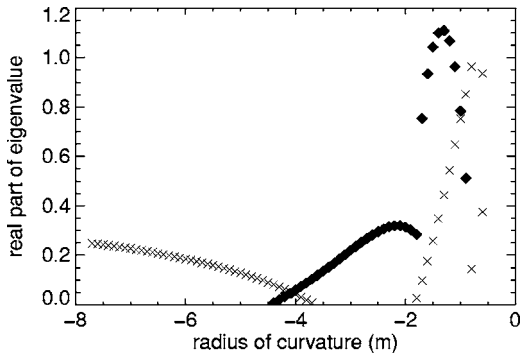

FIG. 8. Positive real parts of eigenvalues of $\nabla\mathcal{N}(\bar{\mathbf{m}})$ in dependency on the phase front curvature of the input light field. Crosses denote eigenvalues connected to the Hopf length scale; solid diamonds denote eigenvalues connected to the length scale of the modulational instability. Parameters as in Fig. 6.

the phase front curvature of the incident light.

For large values of the radius of curvature, i.e., when the system is only weakly changed, the above-described Hopf bifurcation is found. There is a pair of complex conjugate eigenvalues whose real part is positive while the imaginary part is in the order of the Larmor frequency. The latter fact is a clear indication that the observed time dependence is directly related to the Larmor precession. The real part of the pair of eigenvalues decreases when the radius of the phase front curvature is decreased. In an interval of the radius from −4 to −1 m different modes come into play, since they have relatively large real parts of the eigenvalues. The transverse wave numbers, being 25.2 rad/mm at a radius of curvature of −1.3 m, are in line with the length scales of the modulational instability calculated for the homogeneous system or for a linear phase gradient and with the length scale of the experimentally observed stationary hexagonal pattern. The eigenvalues form a resonance-like maximum at a radius of −1.3 m before a Hopf mode with an imaginary part of the eigenvalues being close to the Larmor frequency takes over again if the radius of phase front curvature is further decreased.

It has to be mentioned that the mode with the large wave number occurring for radii between −4 and −1.8 m has complex eigenvalues, i.e., the unstructured state is unstable against the formation of moving targets. The magnitude of the imaginary parts of the eigenvalues, however, is smaller than the Larmor frequency by nearly one order of magnitude. In the experiment stationary hexagons were observed in this range of radii, whose wave numbers agree with those of the targets. This difference is by no means surprising: nonlinear interactions of wave vectors can form hexagons, of course, and these become stationary in a Gaussian beam, if the absolute value of the imaginary part of the eigenvalues is too small. This "locking" phenomenon of hexagons has previously been observed in a closely related experiment involving feedback by a tilted mirror [37]. In the interval of radii from −1.8 to −1 m the eigenvalues are purely real, indicating an instability against stationary target patterns. Obviously, this is compatible with the existence of stationary hexagons.

In Fig. 9 the spatial shape and the temporal evolution of the Hopf mode are illustrated at a radius of curvature of 0.9 m. The dominating length scale is 15.6 rad/mm and the

frequency is approximately 109 kHz. In contrast to the case of flat phase fronts, the motion is directed towards the boundary, which again is in good agreement with the experiment.

VI. CONCLUSION

In the present system, the Gaussian intensity profile of the input laser beam induces nonlinearly a defocusing phase distribution of the light field transmitted by the sodium vapor. In our experiments, this phase distribution is counteracted and even overcompensated by an external focusing phase modulation. Experimentally, we found transitions from radially inwardly moving target patterns and spirals via a stationary hexagonal pattern with a different, significantly smaller length scale to outwardly moving spirals, again with the first length scale.

In a linear stability analysis of the homogeneous system two instabilities are found whose length scales agree with the experimental findings quite well: a Hopf instability at a finite wave number and a modulational instability leading to the formation of a stationary pattern. The modulational instability has the lower threshold in the homogeneous case. It could be shown that an inhomogeneous phase distribution alters the marginal stability curve of the Hopf instability drastically while the threshold of the modulational instability remains nearly unchanged. Hence, in a linear stability analysis with a Gaussian-shaped input intensity profile, the Hopf instability is dominating due to the phase distribution of the nonlinear self-lensing. In further calculations, this self-induced phase modulation is compensated by an antagonistic curvature of the input phase fronts.

Obviously the linear stability analysis used here is much better adapted to experiments using Gaussian beams in the fundamental mode than the usual procedure that assumes plane waves. Due to the assumption of radial symmetry, it can only predict the threshold for the formation of target patterns, of course. From the fact, however, that spontaneous switching between target patterns and spirals is frequently observed, it can be concluded that the threshold of target and spiral pattern formation is not too different. Indeed it should be possible to examine the stability of the system against azimuthal perturbations which lead to spirals. Corresponding efforts are being undertaken at present.

If there is no differentiation between target patterns and spirals, then it can be concluded that the results of the analysis agree very well with the observations. The transitions between different structures for laser beams of various curvatures are nicely reproduced. It turns out that the different sensitivities of the two competing instabilities to phase front curvatures are at the origin of the drastic changes.

Even if experiments are performed with well-collimated laser beams, the phase fronts can be modified nonlinearly. Therefore it can be assumed that in many experiments curved phase fronts come into play. On the other hand, it is shown here that a phase front curvature can have a strong influence on pattern formation and can change the pattern selection completely. Thus it might be wise to study the consequences of phase front curvatures in pattern formation in a wider context.

ACKNOWLEDGMENTS

The authors would like to thank B. Schäpers, G. K. Harkness, G. L. Oppo, and W. J. Firth for fruitful discussions.

[1] A. T. Winfree, Science **175**, 634 (1972).
[2] J. Ross, S. C. Müller, and C. Vidal, Science **240**, 460 (1988).
[3] G. Gerisch, Naturwiss. **58**, 430 (1971).
[4] O. Steinbock, H. Hashimoto, and S. C. Müller, Physica D **49**, 233 (1991).
[5] K. Agladze and O. Steinbock, J. Phys. Chem. **104**, 9816 (2000).
[6] C. Goßen, F.-J. Niedernostheide, and H. G. Purwins, in *Nonlinear Dynamics and Pattern Formation in Semiconductors and Devices*, Vol. 79 of Springer Proceedings in Physics, edited by F.-J. Niedernostheide (Springer, Berlin, 1995).
[7] S. Jakubith, H. -H. Rotermund, W. Engel, A. van Oertzen, and G. Ertl, Phys. Rev. Lett. **65**, 3013 (1990).
[8] M. Assenheimer and V. Steinberg, Nature (London) **367**, 345 (1994).
[9] P. Coullet, L. Gil, and F. Rocca, Opt. Commun. **73**, 403 (1989).
[10] M. Brambilla, F. Battipede, L. A. Lugiato, V. Penna, F. Prati, C. Tamm, and C. O. Weiss, Phys. Rev. A **43**, 5090 (1991).
[11] G. L. Lippi, T. Ackemann, L. M. Hoffer, A. Gahl, and W. Lange, Phys. Rev. A **48**, R4043 (1993).
[12] P. Lodahl, M. Bache, and M. Saffman, Phys. Rev. Lett. **85**, 4506 (2000).
[13] S. A. Akhmanov, M. A. Vorontsov, and V. Y. Ivanov, Sov. Phys. JETP **47**, 707 (1988).
[14] S. A. Akhmanov, M. A. Vorontsov, V. Y. Ivanov, A. V. Larichev, and N. I. Zheleynykh, J. Opt. Soc. Am. B **9**, 78 (1992).
[15] H. Rehn and R. Kowarschik, Opt. Lett. **21**, 1505 (1996).
[16] F. Huneus, B. Schäpers, T. Ackemann, and W. Lange, Appl. Phys. B: Lasers Opt. **B76**, 191 (2003).
[17] F. Huneus, T. Ackemann, and W. Lange, Ukr. J. Phys. **49**, 358 (2004).
[18] Y. Larionova, O. Egorov, E. Cabrera-Granado, and A. Esteban-Martin, Phys. Rev. A **72**, 033825 (2005).
[19] W. J. Firth, J. Mod. Opt. **37**, 151 (1990).
[20] G. D'Alessandro and W. J. Firth, Phys. Rev. Lett. **66**, 2597 (1991).
[21] G. D'Alessandro and W. J. Firth, Phys. Rev. A **46**, 537 (1992).
[22] M. Möller and H. J. Bruns, Rev. Sci. Instrum. **66**, 4535 (1995).
[23] M. Möller, J. P. Seipenbusch, T. Ackemann, B. Schäpers, A. Aumann, A. Gahl, H.-J. Bruns, and W. Lange, Chaos, Solitons Fractals **10**, 675 (1999).
[24] I. Aranson, M. Assenheimer, V. Steinberg, and L. S. Tsimring, Phys. Rev. E **55**, R4877 (1997).
[25] Y. A. Logvin and T. Ackemann, Phys. Rev. E **58**, 1654 (1998).
[26] Z. H. Musslimani and L. M. Pismen, Phys. Rev. A **59**, 1571

(1999).
[27] F. Mitschke, R. Deserno, W. Lange, and J. Mlynek, Phys. Rev. A **33**, 3219 (1986).
[28] T. Ackemann, Y. A. Logvin, A. Heuer, and W. Lange, Phys. Rev. Lett. **75**, 3450 (1995).
[29] T. Ackemann, A. Heuer, Y. A. Logvin, and W. Lange, Phys. Rev. A **56**, 2321 (1997).
[30] B. Schäpers, T. Ackemann, and W. Lange, J. Opt. Soc. Am. B **19**, 707 (2002).
[31] M. Möller and W. Lange, Phys. Rev. A **49**, 4161 (1994).
[32] A. Kastler, J. Opt. Soc. Am. **47**, 460 (1957).
[33] W. Lange and T. Ackemann, Asian J. Phys. **7**, 439 (1998).
[34] W. J. Firth and G. K. Harkness, Asian J. Phys. **7**, 665 (1998).
[35] B. Schäpers, Ph.D. thesis, Westfälische Wilhelms–Universität Münster, 2001.
[36] A. E. Siegman, Opt. Lett. **1**, 13 (1977).
[37] T. Ackemann, B. Schäpers, J. P. Seipenbusch, Y. A. Logvin, and W. Lange, Chaos, Solitons Fractals **10**, 665 (1999).